BJRS

BRAZILIAN JOURNAL
OF
RADIATION SCIENCES
10-03B (2022) 01-27

On the starting and operational transients at the core of the RMB based on 2D multigroup diffusion

Dos Santos R.S.

Comissão Nacional de Energia Nuclear/Instituto de Engenharia Nuclear/SETER, ZIP Code 21941-906, RJ, RJ, Brasil

rsantos@ien.gov.br

ABSTRACT

RMB is a multipurpose reactor to be built by CNEN. As a multipurpose facility, unlike a nuclear power plant, some operations may result in transients, whether during the movement of materials from remote irradiation, extraction of neutrons through beam holes, reactor starting up, control rod accident, etc. For that, a methodology to visualize some variables like neutron fluxes, temperatures, power, etc., was developed. In this one present some preliminary results based on multigroup diffusion theory, thermal hydraulics feedbacks, and numerical methods, systematized in the DINUCLE code. DINUCLE couples a numerical code of multigroup spatial kinetics, for calculations of the flux of neutrons in the core of reactors, with a numerical code for the analysis of thermo hydraulic transients in rods and plates, considering the refrigerant always single-phase. Use was made of a programming in VBA (Visual Basic for Applications) from Excel, for data visualization in the transient.

Keywords: **Multigroup Diffusion, Space Kinetics, Thermal Hydraulics, Data Visualization**

ISSN: 2319-0612
DOI: https://doi.org/10.15392/2319-0612.2022.1993
Submitted: 2022-01-31
Accepted: 2023-06-19

1. INTRODUCTION

RMB is a Brazilian multipurpose reactor designed for radioisotope production, material testing, operation of various neutron beam roles, etc. [1]. As a multipurpose facility, each activity operation can impact core criticality. In this article, we look at some of these operational transients in the core. For that, we modeled it in 2D multigroup spatial kinetic equations, with feedback, through the thermo-hydraulic equation. The expected transients would be the typical start-up of the reactor and those resulting from the introduction of samples to be irradiated, causing disturbances in the criticality of the RMB. The distribution of the neutron flux in the steady state and the transients are calculated numerically. It is worth mentioning that in the case of power reactors, in their operation, the aim is to have a spatial distribution of the neutron flux as flat as possible, avoiding the existence of power density peaks. On the other hand, in the case of RMB, the versatility of its operation seeks a very heterogeneous distribution of the neutron flux, whether for high flux for use in materials testing, in a region of the nucleus, from fast neutrons, as well as for production of radioisotopes, with thermal neutrons, in other regions of the nucleus. Thus, while in a power reactor the result of its operation is the energy delivered in the form of enthalpy, in a reactor such as RMB, its spatial behavior gains relevance, whether operational, reinforced by its visualization of the core of various parameters such as neutron fluxes, temperature distribution, etc. Again, for comparison purposes, usual power reactors operate with minimal excess of reactivity, aiming to have an excess of neutrons that compensates for their operations at nominal temperatures, burning of the fuel throughout their operating cycles, etc. In the case of RMB, this excess of reactivity, due to its multipurpose nature, is much higher, even with much shorter burnup cycles than power reactors. This is mainly related to the fact that, whether for testing materials or for producing radioisotopes, a huge amount of neutrons are demanded in these irradiations. For this, monitoring the criticality state of the RMB, through its reactivity, an equivalent integral parameter, is of fundamental importance for several irradiation operations and sample movement in the RMB core.

2. MATHEMATICAL MODELS

The neutron kinetic equations are given by [2]:

$$\frac{1}{\upsilon_g}\frac{\partial \varphi_g}{\partial t} = \nabla \cdot D_g \nabla \varphi_g - \Sigma_{Rg}\,\varphi_g + \sum_{g' \neq g}^{G} \Sigma_{sg'g}\,\varphi_{g'} + \chi_{pg}(1-\beta)\sum_{g'=1}^{G} \nu_{g'}\,\Sigma_{fg'}\,\varphi_{g'} +$$

$$+ \sum_{k=1}^{I} \chi_{agk}\lambda_k C_k\,, \quad g = 1,2,...,G\,, \tag{1}$$

$$\frac{\partial C_k}{\partial t} = \beta_k \sum_{g'=1}^{G} \nu_{g'}\,\Sigma_{fg'}\,\varphi_{g'} - \lambda_k C_k\,, \quad k = 1,2,...,I\,, \tag{2}$$

where, in a position $\vec{r}$ and time t, $\varphi_g = \varphi_g(\vec{r},t)$ now is the direct neutron flux of energy group g during transients and $C_k = C_k(\vec{r},t)$ is the delayed neutron precursor concentration of group k. The other parameters, υ_g, D_g, Σ_{Rg}, $\Sigma_{sg'g}$, χ_g, ν_g, Σ_{fg} are: velocity, diffusion coefficient, removal macroscopic cross-section, scattering macroscopic cross-section, prompt neutron spectra, neutrons per fission numbers, fission macroscopic cross-section, respectively, of the g-th energy group. For the precursor parameters, χ_{agk}, λ_k, β_k are: delayed neutron spectra, decay constant, delayed neutron fraction, respectively, of the k-th delayed group. Besides, $\beta = \sum_{k=1}^{I} \beta_k$. At any time, and since that ε_g is the energy liberated per fission at the g-th group, the power density is given by:

$$q'''(\vec{r},t) = \sum_{g'=1}^{G} \varepsilon_g\,\Sigma_{fg}(\vec{r},t)\varphi_g(\vec{r},t)\,. \tag{3}$$

The thermal hydraulic model, of an average channel, is given by [3]:

With that, a generic integration along the radius is given by:

$$\rho_m c_m \frac{\partial T_m}{\partial t} = \frac{1}{r^\eta}\frac{\partial}{\partial r} r^\eta K_m \frac{\partial T_m}{\partial r} + q'''_m \quad , \tag{4}$$

having in mind that m means f (fuel) or c (cladding), r distance from center, for a rod $(\eta = 1)$ or for a plate $(\eta = 0)$, and z the axial distance from bottom to top of the channel. $P_m = P_m(r,z,t)$ can represent: ρ_m (density); c_m (specific heat); K_m (conductivity) or q'''_m (heat density). In the cladding T_c represents an average value in the volume without the heat source, $q'''_m = 0$, having in mind the Figure 1.

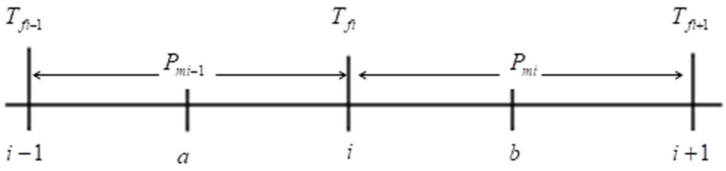

Figure 1: Temperature discretization centered at interface.

For the coolant, we have:

$$\rho_\ell c_\ell \frac{\partial T_\ell}{\partial t} = -\rho_\ell c_\ell \vec{U}.\nabla T_\ell - \nabla.\vec{q}^{"} \quad . \tag{5}$$

Here the properties are associated with the coolant: ρ_ℓ (density); c_ℓ (specific heat); T_ℓ (bulk temperature); $\vec{U}$ (fluid velocity) and $\vec{q}$ (heat flux). Since h_ℓ and $T_{S\ell}$ are the heat transfer coefficient between surface plate/rod to coolant, $\left|\vec{q}^{"}\right| = h_\ell \left(T_{S\ell} - T_\ell\right)$.

A global parameter that gives important information about the reactor deviation from criticality is the reactivity, $\rho(t)$. Considering the direct fluxes and the macroscopic cross-sections time dependent, itis calculate by [4]:

$$\rho(t) = 1 + \frac{\int dV \sum_{g=1}^{G} \varphi_g^* \left[\nabla \cdot D_g \nabla \phi_g - \Sigma_{Rg} \phi_g + \sum_{g' \neq g}^{G} \Sigma_{sg'g} \phi_{g'} \right]}{\int dV \sum_{g=1}^{G} \varphi_g^* \chi_g \left(\sum_{g'=1}^{G} \nu_{g'} \Sigma_{fg'} \phi_{g'} \right)} \quad . \tag{6}$$

Since that, in the steady state, the neutron flux distribution are calculated by using the eigenvalue criticality equation, given by:

$$-\nabla \cdot D_g \nabla \phi_g + \Sigma_{Rg} \phi_g = \frac{1}{\kappa_{ef}} \chi_g \sum_{g'=1}^{G} \nu_{g'} \Sigma_{fg'} \phi_{g'} + \sum_{g' \neq g}^{G} \Sigma_{sg'g} \phi_{g'} \quad . \tag{7}$$

Since here $\varphi_g = \varphi_g(\vec{r}, 0)$, the weight functions are calculated from the following equation [4]:

$$-\nabla \cdot D_g \nabla \phi_g^* + \Sigma_{Rg} \phi_g^* - \sum_{g' \neq g}^{G} \Sigma_{sg \to g'} \phi_{g'}^* = \frac{1}{\kappa_{ef}} \chi_g \Sigma_{fg} \sum_{g'=1}^{G} \chi_{g'} \phi_{g'}^* \quad . \tag{8}$$

At above equation, $\varphi_g^* = \varphi_g^*(\vec{r}, 0)$.

Since that $\varphi_{Ng}(\vec{r},0)$ is the neutron fluxes at nominal condition, normalized power $p(t)$ is given by:

$$p(t)=\frac{\int dV\sum_{g=1}^{G}\varepsilon_g\Sigma_{fg}(\vec{r},t)\varphi_g(\vec{r},t)}{\int dV\sum_{g=1}^{G}\varepsilon_g\Sigma_{fg}(\vec{r},0)\varphi_{Ng}(\vec{r},0)} \quad . \tag{9}$$

These mathematical models are built in a version of the DINUCLE code, a program for transient calculations in reactor cores, for problems in Cartesian geometry, with several energy groups for the prompt neutrons and precursor groups of delayed neutrons [4]. The thermal hydraulic equations are resolved simultaneously with the kinetic equations, in the coolant channels of the fuel plates in the reactor core. In that way, we can consider the feedback effects with the temperatures in the macroscopic cross sections, at the fuel region of the core. In special, in the capture and scattering cross sections, in the attempt of observing the Doppler effect in the fuel and the moderator effect in the coolant.

Part of this work was to develop a computational application for the visualization of spatial results during transients. For this, a program for processing in spreadsheets was developed, using programming in Visual Basic for Applications (VBA) [5].

3. CORE CONFIGURATION AND FEEDBACK EFFECTS

3.1. Core composition and geometry

For purpose of thermal-hydraulics transient analysis at RMB we consider the core composition in Table I:

Table I: Core material composition.

CAPTION	MATERIALS
A	H2O - Pool
B	D2O
C	Aluminum Guide
D	Be - Beryllium
X	Control Rods
F	Ir mini Plate or Dummy Aluminum
G	Fuel Region - U3Si2-Al
I	Core Platform (Matrix Board – Al)
H	Ir MT or Dummy Aluminum
J	H2O – Water Box
L	Al - Chimney

The captions and colors associated with the material regions are given in Figure 2 below:

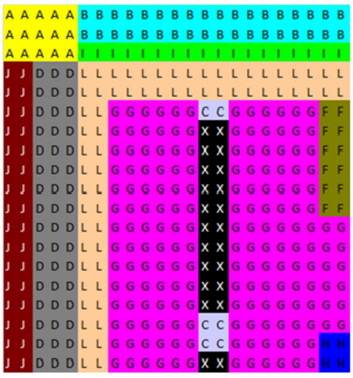

Figure 2: Core material composition caption.

Based on the colors and captions of Figure 2, the configuration of the RMB core is sketched in Figure 3, below:

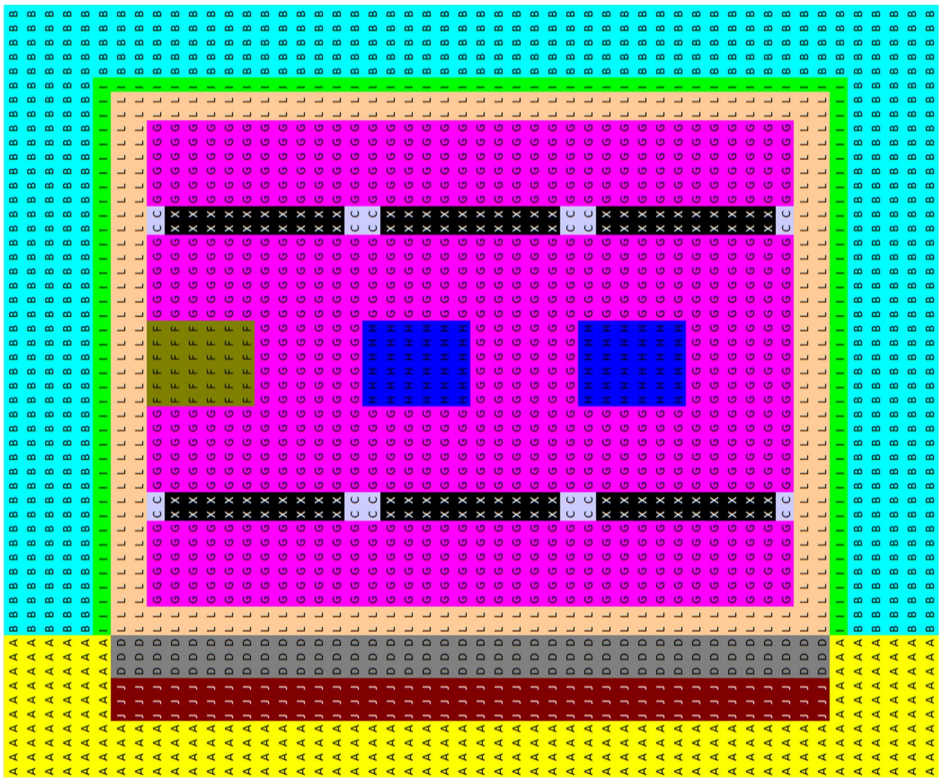

Figure 3: RMB core regions.

3.2. Control rod bank distribution

The banks of control rods are distributed as given by Figure 4, below:

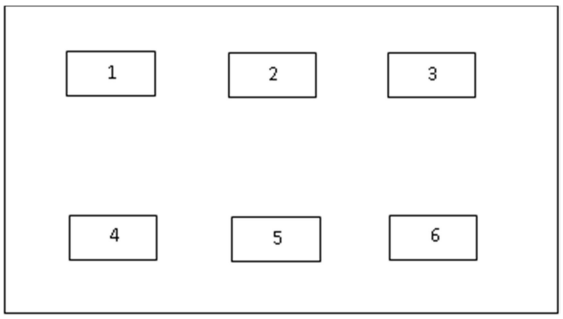

Figure 4: Core control rod distribution.

For our analysis we consider that during the driving of the control rods, the spaces left by them are filled out by water. With that, the following approach was used for calculation of the macroscopic constants:

$$\mathrm{CM} = f.\mathrm{CM_{BC}} + (1\text{-}f).\mathrm{CM_{H2O,}} \tag{10}$$

where, in each energy group, one has:

CM = cross section, diffusion coefficient, etc.;
f = insertion fraction of control rods;
BC = index regarding to the Bank of Control rod;
H2O = index regarding the water of completion of the space left by the absorber rod.

3.3. Feedback effect models

During the transient calculations, the feedback effects are modeled consider the capture macroscopic cross section in the fuel regions follows the resonance integral, for each energy group g, with dependence at temperature T , in Kelvin, like this [2]:

$$\Sigma_{cg}(T) = \Sigma_{cg}(300K)\left[1+\sigma\left(\sqrt{T}-\sqrt{300K}\right)\right] \tag{11}$$

where, σ depend on mass and surface of control rod.

The scattering macroscopic cross section in the moderator region is directly dependent on coolant density:

$$\Sigma_{sg\to g+1}(T_\ell) = \Gamma_{sg\to g+1}(300K)\cdot\rho_\ell(T_\ell) \tag{12}$$

where, $\Gamma_{sg\to g+1}(300K) = \Sigma_{sg\to g+1}(300K)/\rho_\ell(300K)$ is an adjustment multigroup constant and ρ_ℓ is the coolant density.

4. RESULTS AND DISCUSSION

4.1. Validation of DINUCLE

DINUCLE Code is basically the coupling of the CINESP [4] and SIRER [7] Codes. CNESP is a multigroup spatial kinetics program, in Cartesian (x,y) and cylindrical (r,z) geometries, for 1D and 2D problems, for several groups of delayed neutron group precursors, added with the possibility of a Buckling transverse, which allows the simulation of a 3D problem. In the multigroup formulation, the scattering is coupled directly, restricting the scattering to energy groups to lower energies.

When coupled, CINESP is used to calculate the distribution of multigroup fluxes in the spatial nodes from RMB to 2D. With that we generate the values of the peaks of the densities of the powers, based on the RMB nominal power. Once this is done, SIRER module is used to calculate for each node at the core spatial meshes. In this way, assuming the existence of these channels in these nodes, both the temperatures in the cooling channels, as well as the temperatures in the fuel region, will feed back the cross sections, capture in the fuel, as well as the scattering cross sections in the moderator (cooling channel). Thus, the reactor reactivity is a variable generated as a by-product of these calculations. This procedure is repeated at each time interval, performing the RMB transient.

In the validation of the CINESP module, we compared its results with two other codes: MITKIN [8,9] and TWIGL [10]. For this comparison we generate a transient for a heterogeneous, two-dimensional reactor, for two energy groups, caused by the perturbation in the macroscopic capture cross section, in the thermal group. This transient is described in references [8,9]. Table II shows the results generated by CINESP and the other codes, showing the good agreement between the codes.

Table II: Thermal fluxes (A.U.) at different positions and time step of $5x10^{-4}$s.

t(s)	NODE (10,10)				NODE (5,5)		
	MITKIN	TWIGL	CINESP		MITKIN	TWIGL	CINESP
0.00	16.75	16.75	16.75		5.39	5.39	5.39
0.05	18.79	18.79	18.72		6.16	6.15	6.13
0.10	21.75	21.74	21.67		7.25	7.25	7.23
0.15	25.95	25.96	25.86		8.82	8.82	8.78
0.20	32.31	32.37	32.18		11.18	11.20	11.14
0.25	34.12	34.05	33.99		11.80	11.77	11.75

SIRER is a program originally developed for calculating transient temperatures, for square channels of typical PWR rods, also for triangular pin channels typical of liquid metal cooled reactors, and also for plate channels, as is the case of RMB. In SIRER the power density comes from solution of the point kinetic equations. SIRER was validated when used to simulate transients in ADS (Accelerator Driven Systems) proposed in a Benchmark of the NEA - Agency for Nuclear Energy [11]. In this transient, proposed for several laboratories in Europe, the external source of neutrons isinterrupted for a few seconds and resumed again. SIRER has been modified to handle the external source. This version is named SIRER-ADS [12]. Figure 5 shows the result of SIRER-ADS to be compared with the Benchmark, Figure 6. The comparison leaves no doubt that the SIRER module isvery consistent with the other results, qualitatively.

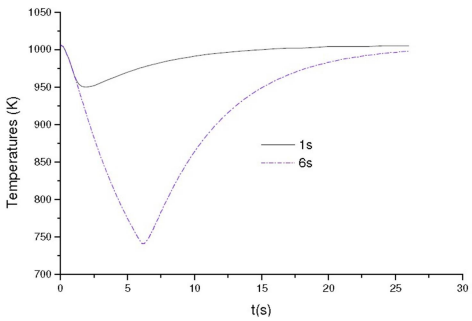

Figure 5 : SIRER-ADS solution.

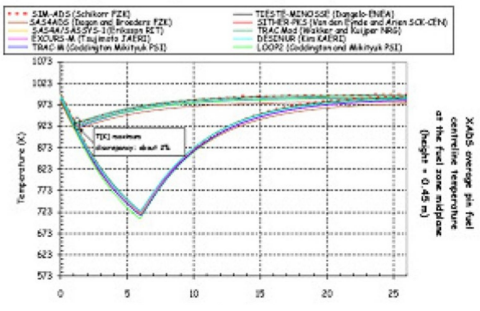

Figure 6 : Benchmark solutions.

To validate the reactivity calculation, Eq. (6), and the normalized power, Eq. (9), we simulate a 1D problem, calculated by the code WIGLE [13], as well as another result from another code, UNICIN [14]. It is a problem using two groups of energies, fast and thermal. Table III shows the results of reactivity and normalized power, the latter not being available for UNICIN. These results show that the CINESP program presents excellent agreement with the other codes for these global

Table III: Reactivity and normalized power.

METHODS	CORE OF 240cm	
	ρ(0.8s)	p(0.8s)
WIGLE	$4.287x10^{-3}$	2.920
CINESP	$4.280x10^{-3}$	2.891
UNICIN	$4.204x10^{-3}$	-

4.2. RMB in steady state operation

At nominal operation, that is, in the steady state, all six control banks are part inserted that in such way that *f=0.5837*. In this configuration, the core criticality is 0.905577. Considering a power of 25 Mw and the design parameters of RMB [1], the thermal (g=4) real flux distribution is given by Figure 7. In this graph it was used the Origin 8.5, a software to analysis and graphing from OriginLab Corporation, released in 2010 [6]. This software has tool to view the graph in perspectives that we can observe the neutron flux from another angle. The data of the macroscopic constants of the energy groups, in addition to the spatial discretization parameters, and the kinetic and channel parameters of the plates, are condensed in the Appendix placed after the references.

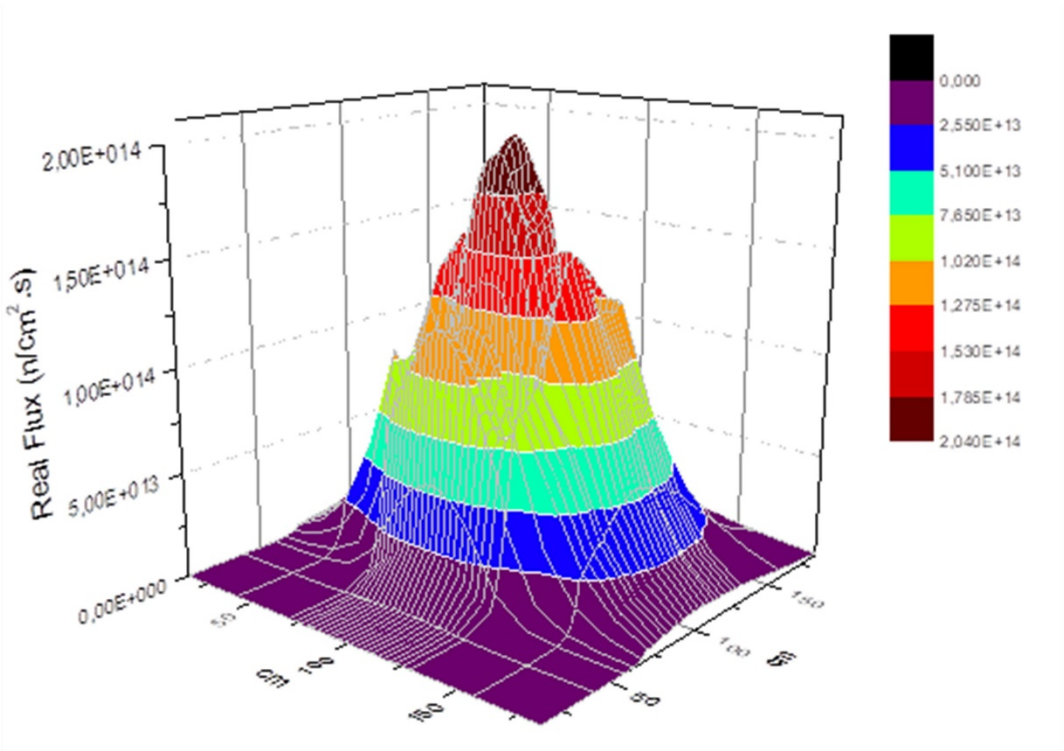

Figure 7: Thermal flux at nominal power in the steady state.

Figure 8 shows the thermal flux from top. It can see that the positions of irradiations elements andthe D2O reflectors exhibit the asymmetry of flux distribution.

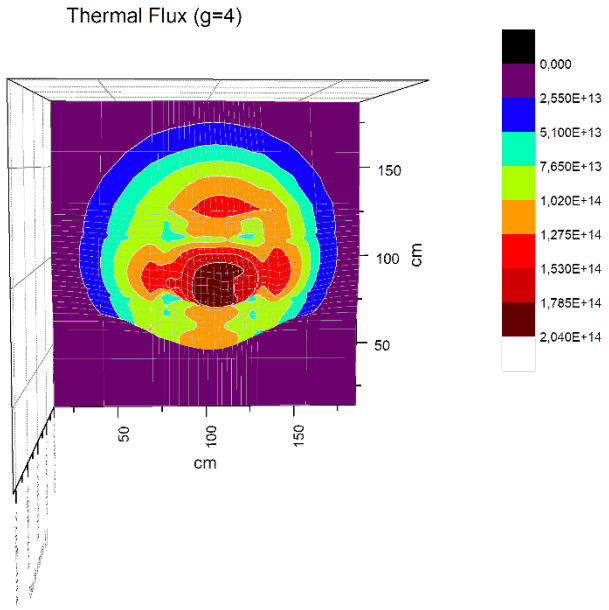

Figure 8: Thermal flux at nominal power in the steady state.

Figure 9 shows the weight function of group four associated to the real flux above.

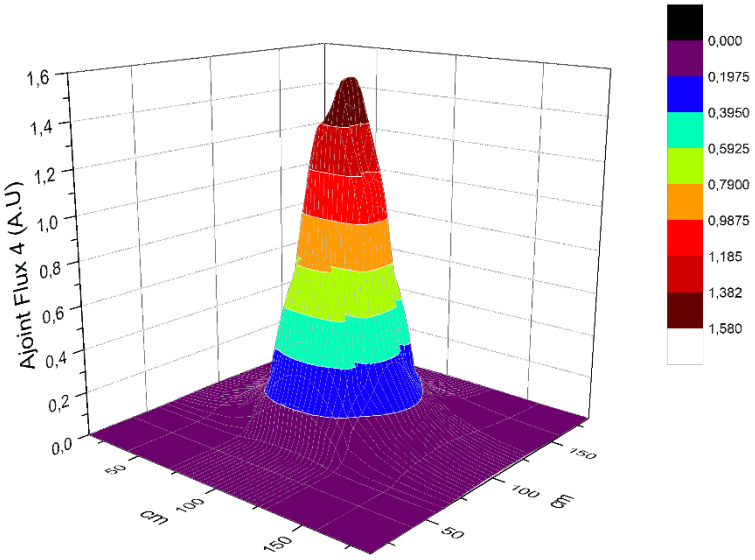

Figure 9: The weight function distribution of group 4.

Figure 10 shows the precursor associated with the delayed neutrons concentration distribution. Note that precursors of delayed neutron do not diffuse through the core.

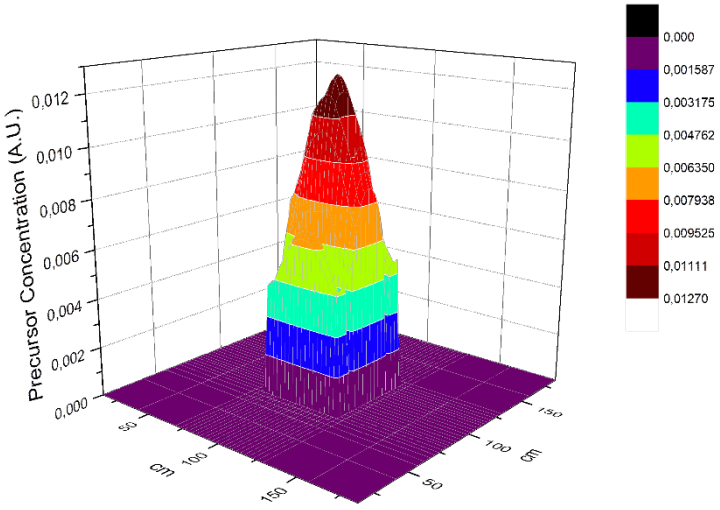

Figure 10: Precursor concentration of delayed neutrons.

Figure 11 shows the centerline temperature distribution associated with the fuel plates.

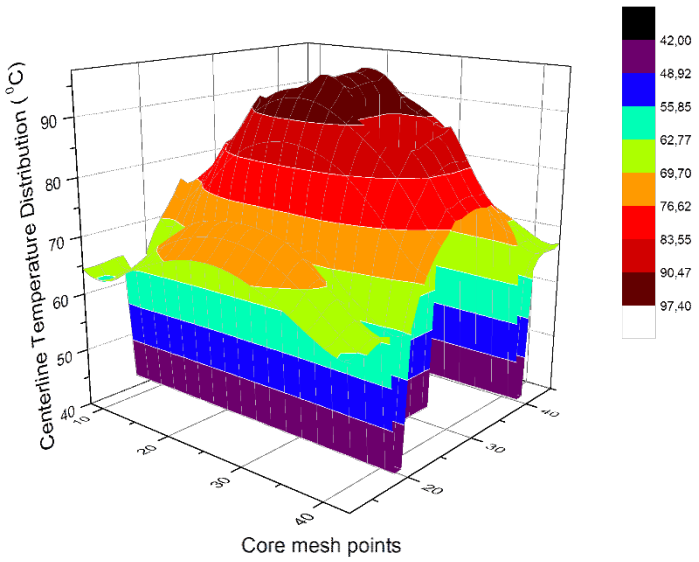

Figure 11: Centerline temperature distribution associated with the fuel plates.

Figure 12 shows the centerline temperature distribution in a view from top. Note that as tempera- tures are calculated on fuel region, irradiation elements, control rods, etc., do not are used at temperature calculations. In this view we can note that temperatures are calculated where there is fuel, consequently, heat.

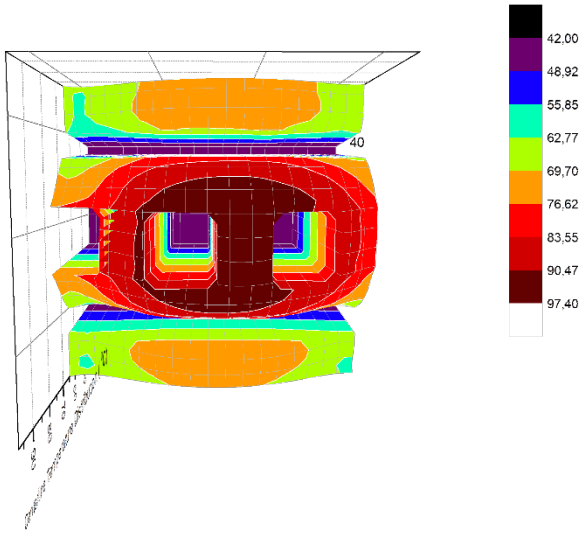

Figure 12: Centerline temperature distribution from top view.

4.3 STARTUP TRANSIENT

The transient begins with the reactor operating in a power of 10^{-13} of the nominal when we simulated the removing the six control banks for 71.15 seconds, when power reaches the nominal value. All six control banks in the core move simultaneity in this hypothetical transient. Since the fuel element has an active height of 61.5 cm and assuming the control rod withdrawal time of 32 seconds, then the rod withdrawal speed is 20 cm per second. This initial condition, called a hot standby condition, core reactor is at temperature of $42^0 C$.

For this transient we used the Excel of Office Software from Microsoft since this platform we can program in Visual Basic for Applications (VBA), to automatize the visualization of the transient simulation. Figure 13 shows the initial thermal flux (g=4).

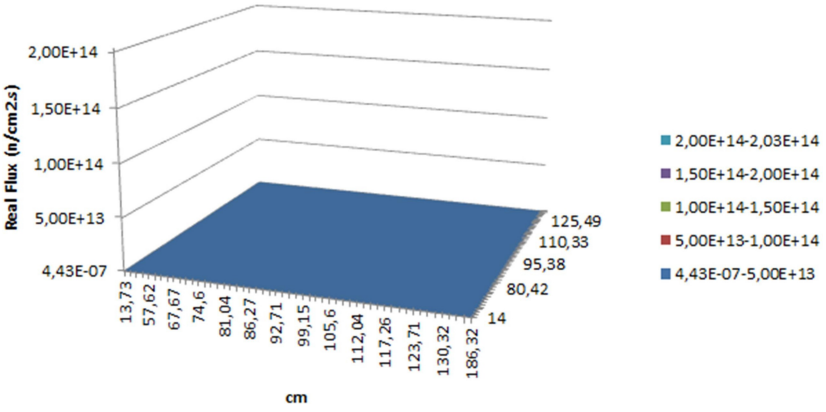

Figure 13: Thermal flux distribution in the initial condition.

Figures 14 to 19 show thermal flux distribution at 68.9, 70.1, 70.4, 70.9, 71.1 and 71.15seconds.

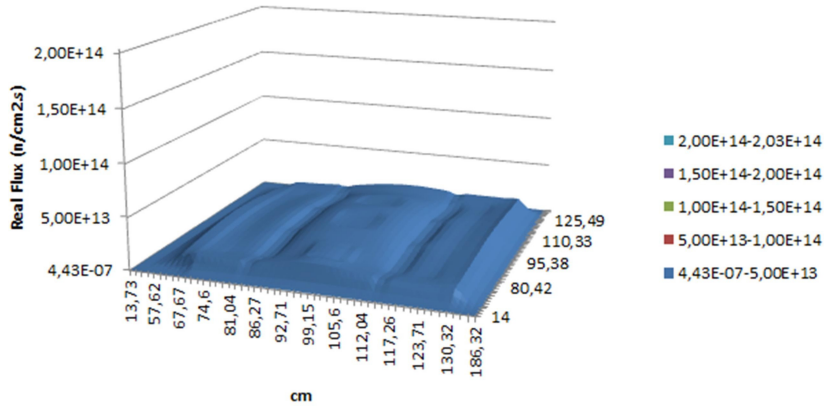

Figure 14: Thermal flux distribution at 68.9 seconds.

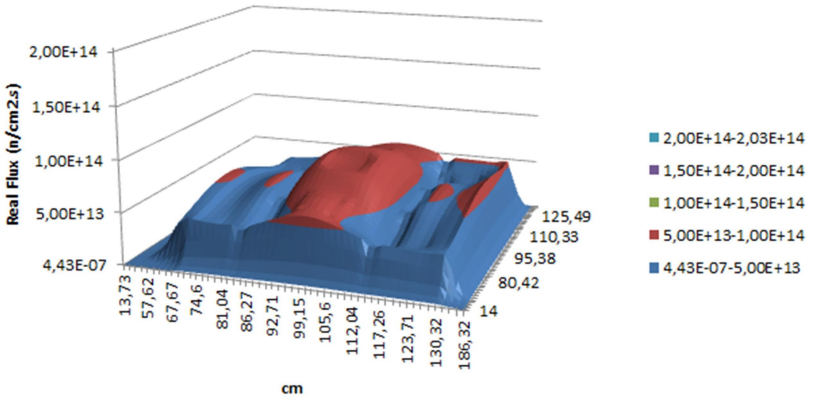

Figure 15: Thermal flux distribution at 70.1 seconds.

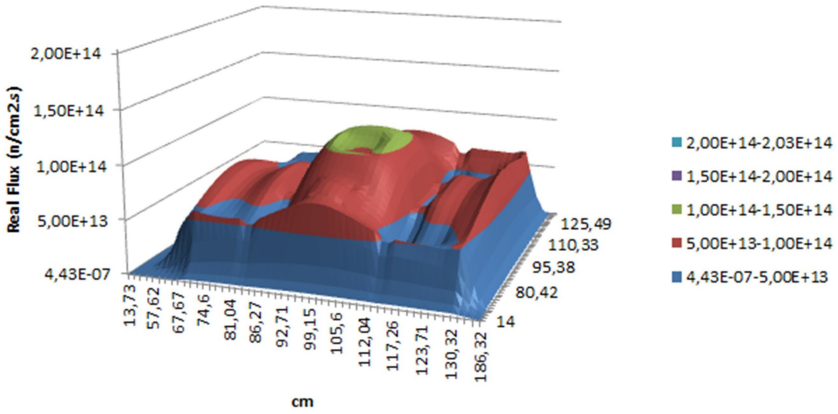

Figure 16: Thermal flux distribution at 70.4 seconds.

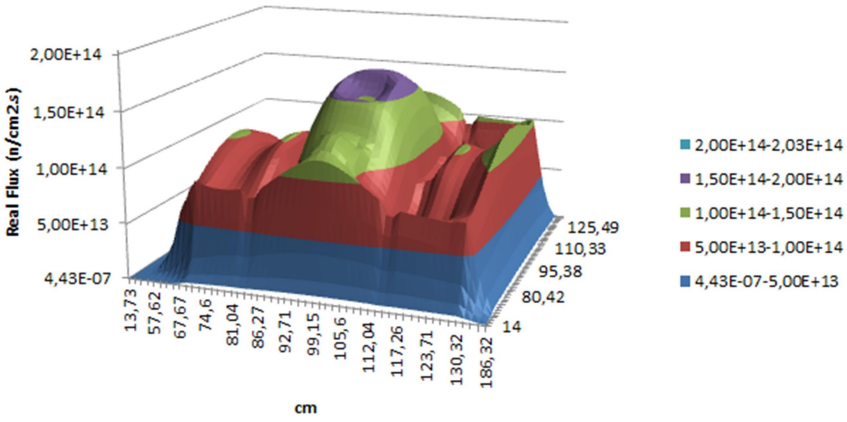

Figure 17: Thermal flux distribution at 70.9 seconds.

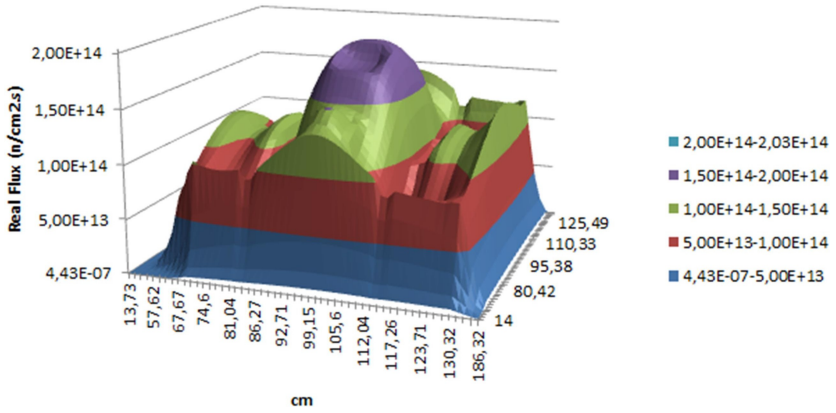

Figure 18: Thermal flux distribution at 71.1 seconds.

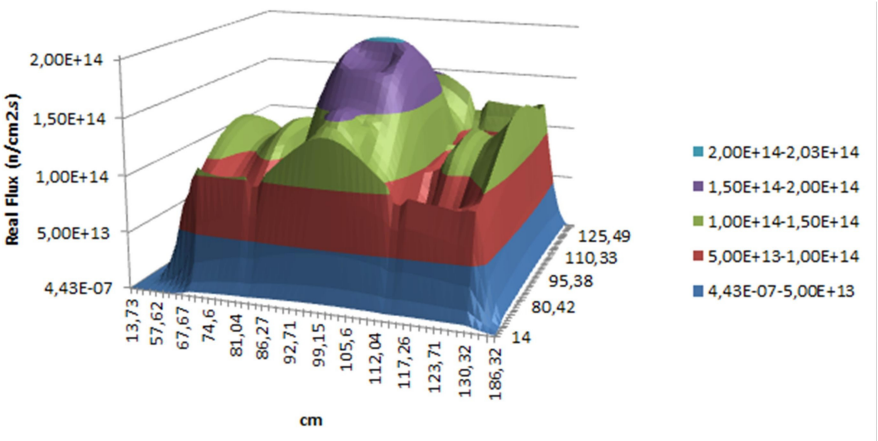

Figure 19: Thermal flux distribution at 71.15 seconds.

Figure 20 shows the centerline temperature distribution at fuel plates at 71.15 seconds.

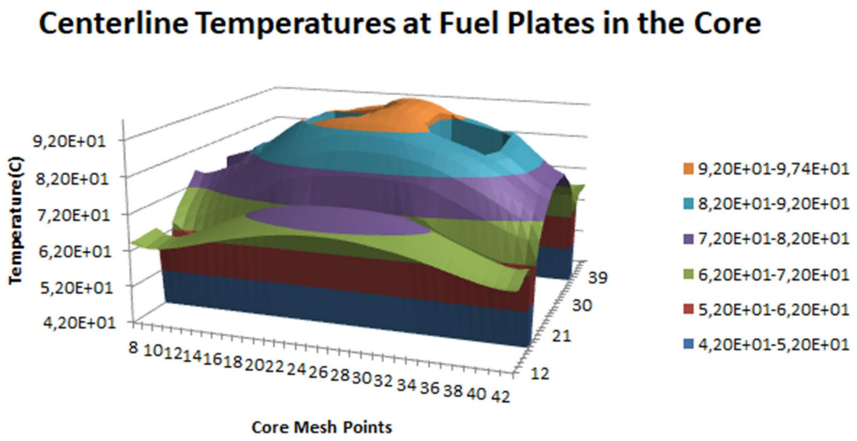

Figure 20: Distribution of fuel centerline temperature at 71.15 seconds.

The behavior of global variables such power and reactivity is showed in Figure 21.

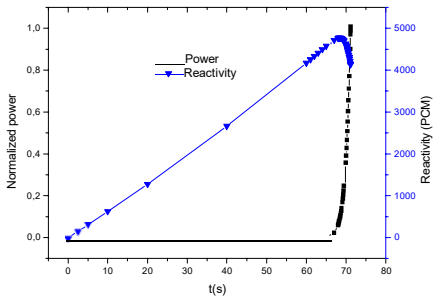

Figure 21: Nominal power and reactivity during 71.15 seconds.

The behavior of the centerline plate fuel temperature (TCL) and outlet channel temperature (TOL), located at maximum flux peak factor, is showed in Figure 22. Figure 23 shows a Zoom of the tran- sient between 65 and 71.15 seconds, to separate the TCL and TOL variations.

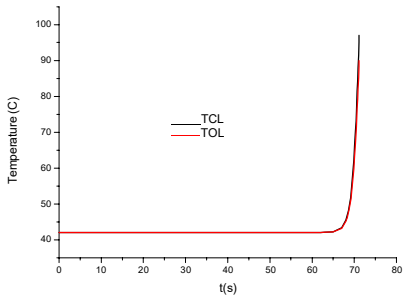

Figure 22: Plate fuel temperature (TCL) and outlet channel temperature (TOL) at maximum flux peak factor, during 71.15 seconds.

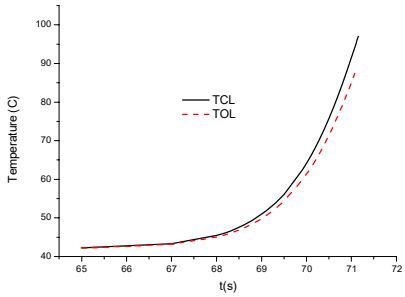

Figure 23: Zoom of plate fuel temperature (TCL) and outlet channel temperature (TOL) at maximum flux peak factor, from 60 seconds.

5. CONCLUSION

The RMB startup transient calculations through the removal of six banks of control rods, brought a 2D spatial visualization of the neutron flux as well as the temperature distributions in the fuel region. In this preliminary analysis, we sought to verify the consistency of spatial views with the mathematical model. In this sense, the results are quite satisfactory. Even for the integral calculations, as reactivity, nominal power, etc. The adopted methodology showed appropriate results for future operational analysis of the RMB, such as, sample movements for irradiation, or even for the analysis of some neutron transients.

REFERENCES

[1] CNEN/DPD/RMB Cálculos iterativos neutrônica/termo-hidráulica para determinar a potência do reator no início de vida. **RMB-10100-RD-007**, 2010.

[2] STACEY, W. M. **Nuclear Reactor Physics**, Second Edition: John Wiley, 2004.

[3] DOS SANTOS, R. S. **Dynamics of Nuclear Reactor Cores based on One and Two-Dimensional Multigroup Diffusion Theory** , X ENFIR, 1995.

[4] DOS SANTOS, R. S. Solução Numérica das Equações da Cinética de Reatores com o Método Explicito de Direções Alternadas (ADE), Comunicação Técnica, **CNEN/IEN-35**, 1992.

[5] MELO, M. AND TOSTES, R. **Criando MACROS com o VBA**, Alta Books Editora, Rio de Janeiro, 2017.

[6] **OriginLab Releases Origin 8.5.1 and OriginPro 8.5.1.** NORTHAMPTON, MA (April 27, 2011). Available at: < Origin 8.5 Press Release (originlab.com)>. Last accessed: January 31, 2022.

[7] **DOS SANTOS, R. S.**, SIRER – Um programa para cálculos de transientes num canal médio do núcleo de reatores, Comunicação Técnica, Instituto de Engenharia Nuclear, Rio de Janeiro, 1995.

[8] **REED, W**. H., **Finite Difference Techniques for the Solution of the Reactor Kinetics Equations**, ScD Thesis, Department of Nuclear Engineering, Massachusetts Institute of Technology, 1969.

[9] **REED, W**. H. AND K. F. HANSEN, A**lternating Direction Methods for the Reactor Kinetics Equations**, Nuclear Science Engineering, 41, 431, 1970.

[10] **YASINSKY, J. B. AND HENRY A. F.**, TWIGL – A Program to Solve the Two-Dimensional, Two-Group, Space-Time Neutron Diffusion Equations with Temperature Feedback, WAPD-TM-743, February, 1968.

[11] **Benchmark on Beam Interruptions in an Accelerator-driven System: Final Report on Phase II Calculations**, http://www.nea.fr/html/science/docs/2004/nsc-doc2004-7.pdf (2004).

[12] **DOS SANTOS, R. S. AND MAIORINO, J. R.**, On the Application of SIRER-ADS in the Simulation of Transients in Accelerator Driven System (ADS), 2007 International Atlantic Conference – INAC 2007, Santos, SP, Brazil, 2007.

[13] **HENRY, A. F. AND A. V. VOTA**, Some Numerical Experiments Concerning Space-Time Reactor Kinetics Behavior, Nuclear Science Engineering, 22, 171, 1965.

[14] **ALCÂNTARA, H. G., PRATI, A., ROSA, M. A. P. AND NAIR, R. P. K.**, Um Código Unidimensional de Solução de Equações de Cinética Multigrupo, 5º ENFIR, 1, 164, Rio de Janeiro, 1985.

APPENDIX A

In this appendix we have the RMB basic data used in this paper. Using Figure 2, the 2D axes are orientated as:

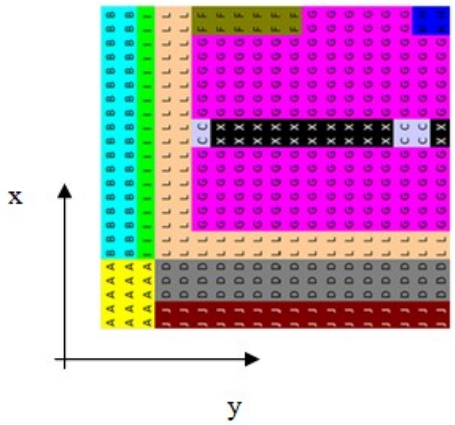

Figure A1: Definition of mesh discretization.

Based on figure A1, the mesh discretization, in cm, are given at Table A1 and Table A2, as follow:

Table A1: Spatial mesh at x direction (DX0 = 13.73)

DX(1) = 13.73;	DX(2) = 13.73;	DX(3) = 13.73;	DX(4) = 2.70;
DX(5) = 2.70;	DX(6) = 2.70;	DX(7) = 2.32;	DX(8) = 2.32;
DX(9) = 2.32;	DX(10) = 1.50;	DX(11) = 1.50;	DX(12) = 1.61;
DX(13) = 1.61;	DX(14) = 1.61;	DX(15) = 1.61;	DX(16) = 1.61;
DX(17) = 1.61;	DX(18) = 1.00;	DX(19) = 1.00;	DX(20) = 1.61;
DX(21) = 1.61;	DX(22) = 1.61;	DX(23) = 1.61;	DX(24) = 1.61;
DX(25) = 1.61;	DX(26) = 1.61;	DX(27) = 1.61;	DX(28) = 1.61;
DX(29) = 1.61;	DX(30) = 1.61;	DX31) = 1.61;	DX(32) = 1.61;
DX(33) = 1.61;	DX(34) = 1.61;	DX(35) = 1.61;	DX(36) = 1.61;
DX(37) = 1.61;	DX(38) = 1.00;	DX(39) = 1.00;	DX(40) = 1.61;
DX(41) = 1.61;	DX(42) = 1.61;	DX(43) = 1.61;	DX(44) = 1.61;
DX(45) = 1.61;	DX(46) = 1.50;	DX(47) = 1.50;	DX(48) = 2.00;
DX(49) = 14.00;	DX(50) = 14.00;	DX(51) = 14.00;	DX(52) = 14.00;
DX(53) = 14.00;			

Table A2: Spatial mesh at y direction (DY0 = 14.00)

DY(1) = 14.00;	DY(2) = 14.00;	DY(3) = 14.00;	DY(4) = 14.00;
DY(5) = 2.00;	DY(6) = 1.50;	DY(7) = 1.50;	DY(8) = 1.30;
DY(9) = 1.37;	DY(10) = 1.37;	DY(11) = 1.37;	DY(12) = 1.37;
DY(13) = 1.37;	DY(14) = 1.37;	DY(15) = 1.37;	DY(16) = 1.37;
DY(17) = 1.37;	DY(18) = 1.37;	DY(19) = 1.30;	DY(20) = 1.30;
DY(21) = 1.37;	DY(22) = 1.37;	DY(23) = 1.37;	DY(24) = 1.37;
DY(25) = 1.37;	DY(26) = 1.37;	DY(27) = 1.37;	DY(28) = 1.37;
DY(29) = 1.37;	DY(30) = 1.37;	DY(31) = 1.30;	DY(32) = 1.30;
DY(33) = 1.37;	DY(34) = 1.37;	DY(35) = 1.37;	DY(36) = 1.37;
DY(37) = 1.37;	DY(38) = 1.37;	DY(39) = 1.37;	DY(40) = 1.37;
DY(41) = 1.37;	DY(42) = 1.37;	DY(43) = 1.30;	DY(44) = 1.50;
DY(45) = 1.50;	DY(46) = 2.00;	DY(47) = 14.00;	DY(48) = 14.00;
DY(49) = 14.00;	DY(50) = 14.00;	DY(51) = 14.00;	

The multigroup constants are given in the following tables, assuming four groups:

Table A3: Velocity, spectrum and neutron per fission, at the energy groups.

g	$\upsilon_g\,(cm/s)$	χ_g	ν_g
1	.1915E+10	.7432E+00	2.7325E+00
2	.3821E+09	.2566E+00	2.4445E+00
3	.5167E+07	.2200E-03	2.4190E+00
4	.3072E+06	.0000E+00	2.4188E+00

Table A4: Macroscopic cross-sections (cm^{-1}), diffusion coefficient (cm), at energy group g=1.

GROUP 1					
I	Σ_{ag}	Σ_{fg}	D_g	$\Sigma_{s1\to2}$	MATERIAL(I)
1	.4310E-03	.0000E+00	.1948E+01	.1077E+00	H2O - Pool
2	-.6937E-04	.0000E+00	.1867E+01	.9282E-01	D2O
3	.2469E-03	.0000E+00	.2473E+01	.3134E-01	Aluminum Guide
4	.3513E-02	.0000E+00	.1572E+01	.4033E-01	Be - Beryllium
5	.1077E-02	.0000E+00	.2015E+01	.7822E-01	Control Rods
6	.3871E-03	.0000E+00	.2310E+01	.3123E-01	Ir mini Plate or Dummy Al
7	.4126E-03	.3717E-03	.2137E+01	.7288E-01	Fuel Region (U3Si2-Al)
8	.3871E-03	.0000E+00	.2310E+01	.3123E-01	Matrix Board - Al
9	.3871E-03	.0000E+00	.2310E+01	.3123E-01	Ir MT or Dummy Al
10	.4310E-03	.0000E+00	.1948E+01	.1077E+00	H2O – Water Box
11	.3871E-03	.0000E+00	.2310E+01	.3123E-01	Al - Chamine

Table A5: Macroscopic cross-sections (cm^{-1}), diffusion coefficient (cm), at energy group g=2.

GROUP 2					
I	Σ_{ag}	Σ_{fg}	D_g	$\Sigma_{s2\to3}$	MATERIAL(I)
1	.9859E-05	.0000E+00	.1050E+01	.1477E+00	H2O - Pool
2	.1282E-06	.0000E+00	.1157E+01	.3572E-01	D2O
3	.1479E-03	.0000E+00	.1483E+01	.2118E-01	Aluminum Guide
4	.5263E-04	.0000E+00	.7632E+00	.2091E-01	Be - Beryllium
5	.5057E-02	.0000E+00	.1112E+01	.8305E-01	ControlRods
6	.3871E-03	.0000E+00	.2310E+01	.3123E-01	Ir mini Plate or Dummy Al
7	.2751E-03	.2091E-03	.1165E+01	.8585E-01	Fuel Region (U3Si2-Al)
8	.3871E-03	.0000E+00	.2310E+01	.3123E-01	Matrix Board - Al
9	.3871E-03	.0000E+00	.2310E+01	.3123E-01	Ir MT or Dummy Al
10	.9859E-05	.0000E+00	.1050E+01	.1477E+00	H2O - Water Box
11	.8838E-03	.0000E+00	.1018E+01	.1307E-01	Al - Chamine

Table A6: Macroscopic cross-sections (cm^{-1}), diffusion coefficient (cm), at energy group g=3.

	GROUP 3				
I	Σ_{ag}	Σ_{fg}	D_g	$\Sigma_{s3\to4}$	MATERIAL(I)
1	.9997E-03	.0000E+00	.5774E+00	.1447E+00	H2O - Piscina
2	.1523E-05	.0000E+00	.1224E+01	.1555E-01	D2O
3	.5410E-03	.0000E+00	.2199E+01	.1390E-01	GUIA ALUMINIO
4	.2292E-03	.0000E+00	.6165E+00	.2201E-01	Be - Berilio
5	.1228E+00	.0000E+00	.6437E+00	.4718E-01	BC
6	.3871E-03	.0000E+00	.2310E+01	.3123E-01	Ir mini Plate or Dummy Al
7	.7456E-02	.3358E-02	.8630E+00	.7854E-01	Fuel Region (U3Si2-Al)
8	.3871E-03	.0000E+00	.2310E+01	.3123E-02	Matrix Board - Al
9	.3871E-03	.0000E+00	.2310E+01	.3123E-01	Ir MT or Dummy Al
10	.9997E-03	.0000E+00	.5774E+00	.1447E+00	H2O - Water Box
11	.5014E-02	.0000E+00	.1002E+01	.8836E-02	Al - Chamine

Table A7: Macroscopic cross-sections (cm^{-1}), diffusion coefficient (cm), at energy group g=4.

	GROUP 4				
I	Σ_{ag}	Σ_{fg}	D_g	–	MATERIAL(I)
1	.1874E-01	.0000E+00	.1507E+00	.0000E+00	H2O - Piscina
2	.2958E-04	.0000E+00	.8766E+00	.0000E+00	D2O
3	.8117E-02	.0000E+00	.1280E+01	.0000E+00	GUIA ALUMINIO
4	.3907E-02	.0000E+00	.6177E+00	.0000E+00	Be - Berilio
5	.4217E+00	.0000E+00	.2995E+00	.0000E+00	BC
6	.5354E-02	.0000E+00	.8861E+00	.0000E+00	Ir mini Plate or Dummy Al
7	.2355E-01	.4793E-01	.3005E+00	.0000E+00	Fuel Region (U3Si2-Al)
8	.5354E-02	.0000E+00	.8861E+00	.0000E+00	Matrix Board - Al
9	.5354E-02	.0000E+00	.8861E+00	.0000E+00	Ir MT or Dummy Al
10	.1874E-01	.0000E+00	.1507E+00	.0000E+00	H2O - Water Box
11	.5354E-02	.0000E+00	.8861E+00	.0000E+00	Al - Chamine

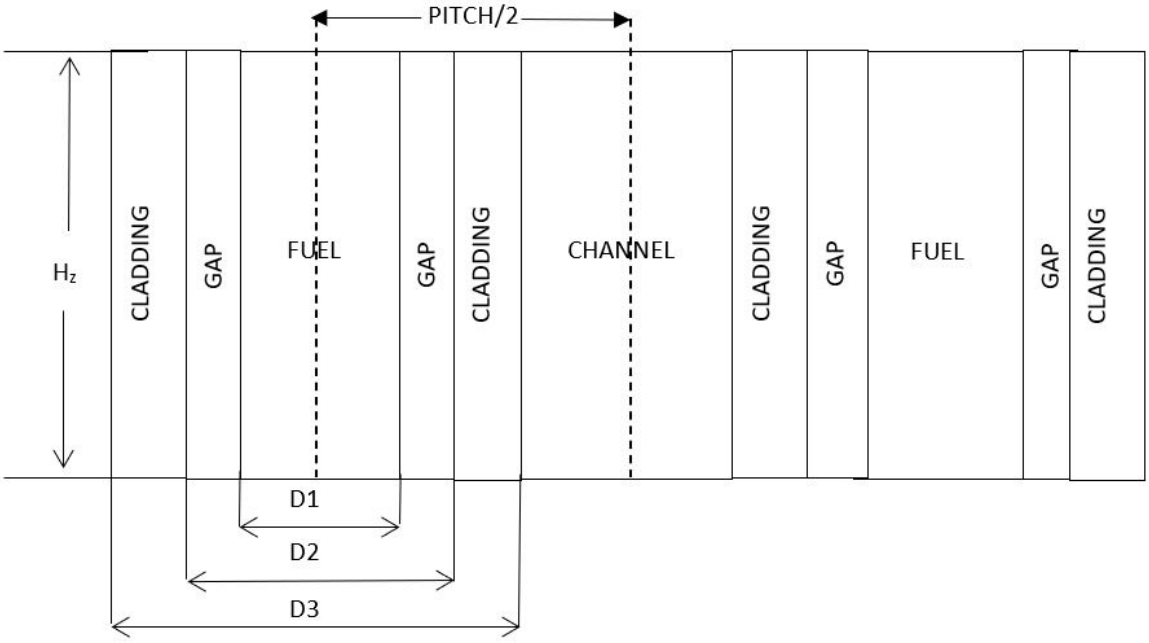

Figure A2: Definition of channel dimensions.

Based on figure A2, for plate fuel, D2=D1=0.135cm, D3=0.331cm and PITCH=0.3833cm. Each plate has an active length (H_Z) of 61.5cm and a width of 6.5cm. In all calculations a delayed neutron precursor group with β=0.0075 and a decay constant λ=0.08s^{-1} was used. The core of the RMB contains 27 fuel elements in the form of plates, at a rate of 21 plates per element. The mass flow through the fuel elements is 720kg/s. For the transient, both in the neutron kinetics equations and in the thermos hydraulic equations, a time step of 0.0025 second was used. The term associated with the transverse neutron escape, aiming the 3D representation, is represented by the geometric Buckling. $B^2=(\pi/H_Z)^2=2.6439x10^{-3}cm^{-2}$, for all energy groups.